

(Supplementary materials)

Numerical Study on the Flow and Heat Transfer Coupled in a Rectangular Mini-Channel by Finite Element Method for Industrial Micro-Cooling Technologies

Claude Aurélien KAMDEM KAMDEM ¹ and Xiaolu ZHU ^{1,2,3,*}

¹ College of Mechanical & Electrical Engineering, Hohai University, Changzhou 213022, China; kamdemclaude2020@outlook.com

² Changzhou Key Laboratory of Digital Manufacture Technology, Hohai University, Changzhou 213022, China

³ Jiangsu Key Laboratory of Special Robot Technology, Hohai University, Changzhou 213022, China

* Correspondence: zhuxiaolu@hhu.edu.cn; Tel.: +86-1586-186-3691

Received: 30 July 2020; Accepted: 31 August 2020; Published: 3 September 2020

1. Materials and Methods

Table S1 describes the comparison of the current state-of-the-art for heat transfer.

Table S1. Comparison of the current state-of-the-art for heat transfer. Notation: Data not available (NA)

Authors	Geometry	Fluid	Flow direction	Dh (mm)	V (m/s)	T _{inlet} (°C)	T _{wall} (°C)	T _{sat} (°C)	Heating method material	Heat flux	Heat load power P _{max} (W)
Present work	Rectangular	Liquid / gas (water)	Vertical/horizontal	0.5	0.25	20	150	100	Copper	1.02 - 5.34 MW/m ²	NA
K. Deepak et al.[1]	Square	Ferrofluid	Up/down, left/right	NA	NA	25	180	144	(MnNiSi)0.7(Fe2Ge)0.3	NA	1.5
M.S. Pattanai, et al.[2]	Concentric torus × 3	Iron oxide: oil	Axial/radial	25	NA	20	580	NA	Silicone	NA	1000
H. Ganapathy et al.[3]	Rectangular	R134a	Horizontal	0.1	NA	NA	27	39.39	NA	200 to 800 kW/m ²	NA
Karayianis et al. [4]	Rectangular	Water	Horizontal	0.561	NA	NA	120-135	105	copper	480 - 500 kW/m ²	NA
Mengnan Li,	cubic	water	horizontal	1.2	1 × 10 ⁻⁴	102.5	90 - 110	100	NA	12444 W/m ²	NA

Igor A.
Bolotno
v [5]
Zhuan
et al.[6]

Circular	R134a / R22	horizonta 1	0.5	NA	3	NA	30	NA	50 - 129 kW/m ²	NA
----------	----------------	----------------	-----	----	---	----	----	----	-------------------------------	----

1.1 Laminar flow

Thus, Figure S1 shows a brief appearance of monophasic flow in a rectangular section channel.

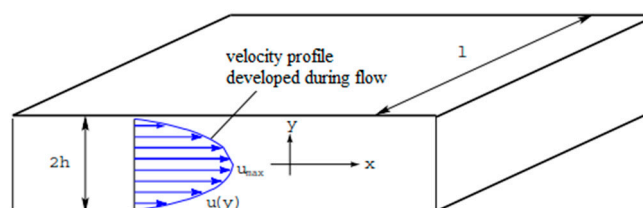


Figure S1. Monophasic flow in a rectangular section channel.

From the momentum conservation equation, it has been demonstrated that for such a viscous and incompressible flow. The velocity distribution across the cross-section of the rectangular channel is as follows [7]:

$$u(y) = -\frac{dp}{dx} \frac{h^2}{2\mu} \left[1 - \left(\frac{y}{h} \right)^2 \right] \tag{1}$$

Here, h denotes the half-height of the channel. The laminar distribution is parabolic and known as "Poiseuille's Profile." Supposing $y = 0$, the maximum velocity of the flow is [7]:

$$u_{\max} = -\frac{dp}{dx} \frac{h^2}{2\mu} \tag{2}$$

with $A = 2h \cdot l$ (the channel section area) and knowing that the average velocity is [7]:

$$Q_v = u_{\text{avg}} \cdot A \tag{3}$$

$$\text{and } Q_v = \int_{-h}^{+h} u(y) \cdot dA \tag{4}$$

Therefore, the relationship between the maximum flow velocity and its average velocity [7]:

$$u_{\text{avg}} = \frac{2}{3} u_{\max} \tag{5}$$

According to Figure S1, the pressure drop in two points, for example, X_1 and X_2 , is [7]:

$$\Delta P = u_{\text{avg}} \frac{3\mu}{h^2} \Delta X \tag{6}$$

The balance of the forces applied to an elementary volume of a Poiseuille flow fluid shows that the tangential force along the direction of the flow, which is exerted between the layers of the fluid, is constant. So, it is called τ the corresponding viscous stress [7]:

$$\tau = \mu \cdot \frac{\partial u}{\partial y} \tag{7}$$

Thus occurs as a linear function of y occurs while reaching its maximum value at the wall τ_{wall} noted the parietal stress is related to the longitudinal pressure gradient [8]:

$$\tau_{wall} = \mu_{wall} \cdot \left(\frac{\partial u}{\partial y} \right)_{wall} = \frac{\Delta P \cdot D_h}{4 \cdot L} \quad (8)$$

where the index wall indicates that the viscosity is that of the fluid at the temperature T_{wall} of the wall. The hydraulic diameter in our case is given by [9]:

$$D_h = \frac{4 \cdot h \cdot l}{2h + l} \quad (9)$$

where h is considered half of the channel height. The coefficient of parietal friction is given by the following dimensionless number [7]:

$$c_f = \frac{2\tau_p}{\rho \cdot u_{avg}^2} \quad (10)$$

where ρ and u_{avg} are the values of the density and the average velocity of the flow, respectively.

1.2 Number of theoretical Poiseuille

In the case of two semi-infinite parallel flat plates, α tends to zero and the preceding formula is thus reduced to [9]:

$$c_f = \frac{24}{\text{Re}_{Dh}} \quad (11)$$

Depending on the geometry of the channel, the number of theoretical Poiseuille Po_{th} is the product of the Reynolds number and the friction factor which is equal to 24, so this number is constant [9]:

$$Po_{th} = c_f \cdot \text{Re}_{Dh} = 24 \quad (12)$$

where Re_{Dh} represents the Reynolds number based on the hydraulic diameter of the channel [10]:

$$\text{Re}_{Dh} = \frac{\rho \cdot V \cdot D_h}{\mu} \quad (13)$$

and the flow friction factor, C_f is defined by [11]:

$$C_f = \frac{D_h \Delta P}{2\rho U^2 L} \quad (14)$$

where L is the channel length, and U is the mean flow velocity. The hydrodynamic section length L_h for rectangular microchannels is defined by the following expression [12]:

$$L_h = 0.05 \cdot \text{Re} \cdot D_h \quad (15)$$

1.3 Simulation parameters

The liquid used temperature was ranged from 22 to 44°C and liquid velocities, ranging from 0.25 to 12 m/s [9]. The measurements were relied on using capillary tubes to determine kinematic viscosity and viscosity dynamic corresponding to the following values: $\nu = 1,043.10^{-6} m^2 / s$ and $\mu = 1,040.10^{-3} kg / m.s$ [13]. These studies revealed that at a temperature of 20°C the density of the water was $\rho = 997.77 kg / m^3$, and the corresponding formula was [14]:

$$\rho(T) = 1001 - 9,084.10^{-2} T - 3,416.10^{-3} T^2 \quad (16)$$

Previously, the work has been done using the flow rates at 450 ml/min for a velocity vector with an equal maximum velocity of 0.8577048 m/s, and 850 ml/min for a velocity vector with an equal maximum velocity of 1.6205020 m/s [8]. So theoretically, the velocity is also high when the flow rate grows, and the simulation results in Table S2 were obtained in laminar flow:

Table S2. Values of the simulation data [8]

Parameters	Value
Hydraulic diameter	Dh= 9.807E-01mm
Reynold's number	Rey=5.556E+02
Fluid Flow rate	DEN= 1000E+00
Dynamic viscosity	VIS=1.041E-03Kg/m.s

Given these obtained values, the inlet velocity can be calculated by applying:

$$Re_{Dh} = \frac{\rho \cdot V \cdot Dh}{\mu} \implies V_e = \frac{R_e \cdot \mu}{\rho \cdot Dh} \implies V_e = \frac{5.556E+02 \times 1.041E-03}{997.7 \times 0.9807E-03} = 0.5915m^{s^{-1}}$$

So, for the channel with the hydraulic diameter of 0.98mm, the inlet velocity corresponding was 0.6 m/s.

The parameters in Table S3 were used in the laminar flow [7]:

Table S3. Values of the simulation Parameters [7]

Qv [ml/min]	Ve [m/S]	Re	V _{moy} Sim[m/s]	C _f (sim)	C _f (theo)
850,6	0,282035	1030	2,017846	0,00820	0,023307
1300	0,431044	1574	2,975100	0,00625	0,015250

1.4 Mesh

Table S4 provides supporting data for mesh validation.

Table S4. Supporting data for mesh validation.

Type of mesh	Domain elements	Static pressure in 0.5mm, V=0.25m/s (Pa)
Extremely fine	130311	1.72 X10 ³
Extra fine	41757	1.72 X10 ³
Finer	13036	1.72 X10 ³
Fine	9107	1.76 X10 ³
Normal	6669	1.7 X10 ³
Coarse	3562	1.68 X10 ³
Coarser	2336	1.59 X10 ³
Extra coarse	1323	1.36 X10 ³
Extremely coarse	1039	1.1 X10 ³

Figure S2 presents the graph of the data for the mesh validation to demonstrate the accuracy of the simulation based on the static pressure. It is found that the mesh is independent.

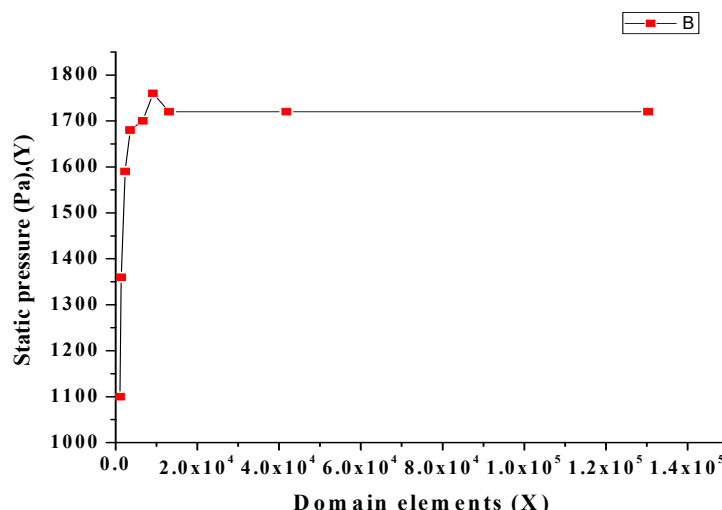


Figure S2. Supporting data for mesh validation

2. Results and Discussions

2.1 Two-phase flow heat transfer at constant wall temperature in the approximative model

Table S5 presents the different data recorded during the simulation in the horizontal direction at a different position along the channel

Table S5. Data along the channel at different horizontal position

Case 1: Two-phase flow heat transfer at the constant wall temperature						
Time: 0s						
Position (mm)	A: X= -71	B: X= -41	C: X= 10	D: X= 31	E: X= 61	F: X= 72.4
	Y= -30.8	Y= -30.8	Y= -30.8	Y= -30.8	Y= -30.8	Y= -30.8
Temperature (K)	293.15	293.15	293.15	293.15	293.15	293.15
Time: 0.45s						
Position (mm)	A: X= -71	B: X= -41	C: X= -1	D: X= 31	E: X= 61	F: X= 72.4
	Y= -30.8	Y= -30.8	Y= -30.8	Y= -30.8	Y= -30.8	Y= -30.8
Temperature (K)	293.17	372.44	375.93	372.10	371.52	356.22
Time: 1.1s						
Position (mm)	A: X= -71	B: X= -41	C: X= -1	D: X= 31	E: X= 61	F: X= 72.4
	Y= -30.8	Y= -30.8	Y= -30.8	Y= -30.8	Y= -30.8	Y= -30.8
Temperature (K)	293.45	372.12	374.67	376.36	373.58	346.29

It is also necessary to determine the exact value of the Reynolds number:

$$Re_{Dh} = \frac{\rho \cdot V \cdot D_h}{\mu} = \frac{1000 \times 0.30 \times 1 \times 10^{-3}}{0.001} \approx 300$$

2.2 Determination of the dissipated heat flux for different application areas, the convective heat transfer coefficient, and the fin efficiency of the rectangular mini-channel

Several studies have been conducted on the determination of the value of the convective heat transfer coefficient. According to these investigations, Table S6 gives the approximate values of the convective heat transfer coefficients that have been summarized [15]. The same table afterward was used in situations with microchannels heat sinks [16].

Table S6. Approximate values of convection heat transfer coefficients [15]

Mode	$h(w/m^2 \cdot c)$
Free convection, air	5-25
Forced convection, air	10-500
Forced convection, water	100-15000
Pool boiling, water	25000-35000
Flow boiling, water	5000-100000

These obtained values from the calculation of the efficiency and the convective heat transfer coefficient are plotted in Figure S3 to express the relationship between the convective heat transfer coefficient and efficiency.

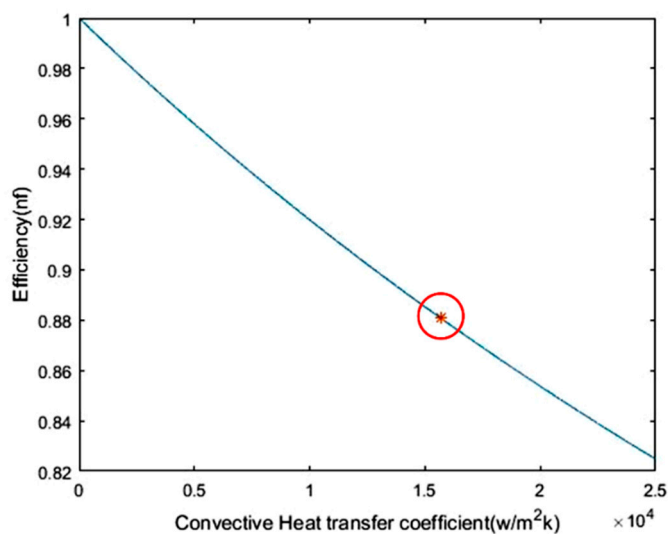


Figure S3. Relationship between the convective heat transfer coefficient and efficiency.

Figure S4 shows the flow boiling effects with the copper wall sets as a material for all the boundaries of the rectangular mini-channel with increasing temperature at the top and bottom walls of the channel.

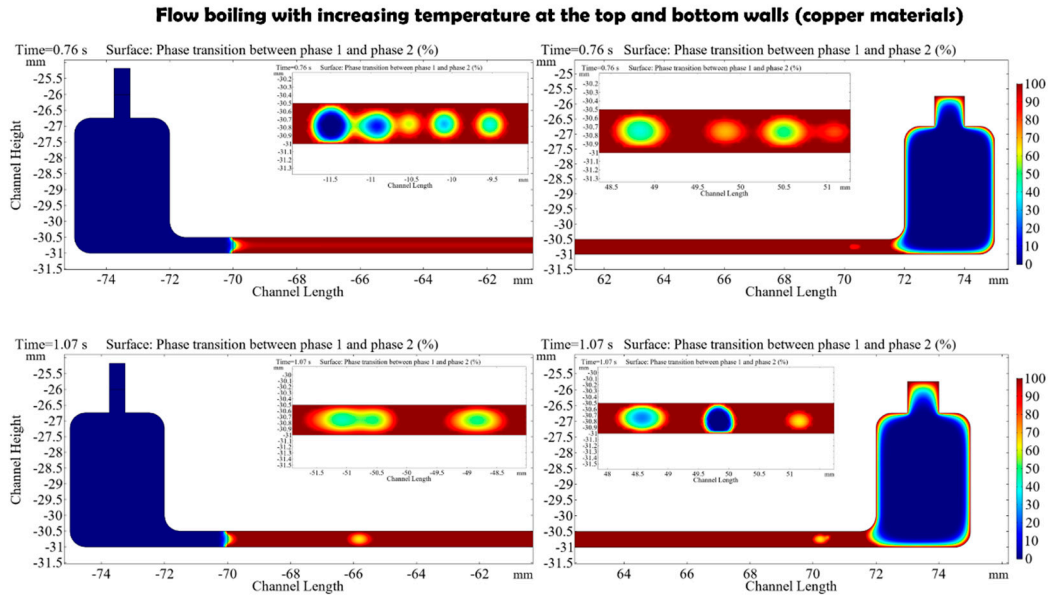


Figure S4. Flow boiling with increasing temperature (copper wall materials)

2.3 The pressure, velocity, and temperature distribution in the microflow with increasing and decreasing temperature along the top and bottom walls considering phase change inside the channel in the phase-field

Figure S5 presents the graph of temperature vs. time for the different wall materials at the same velocity.

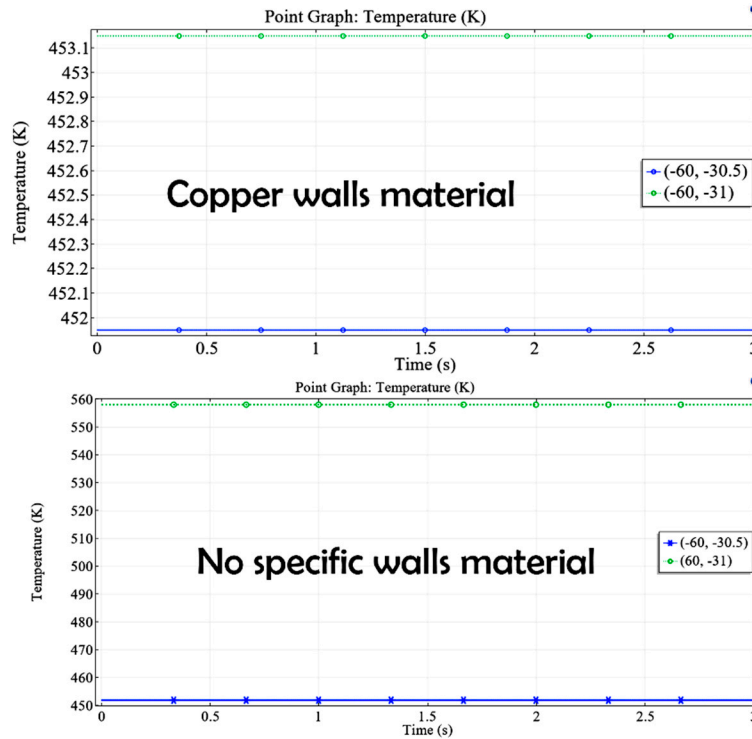


Figure S5. Graph of the temperature VS time with different wall materials at the same velocity.

Figure S6 shows the graph of temperature vs. time when $v=0$, and $v \neq 0$ with the same material at the walls. In both situations, the temperature behaves the same versus the time.

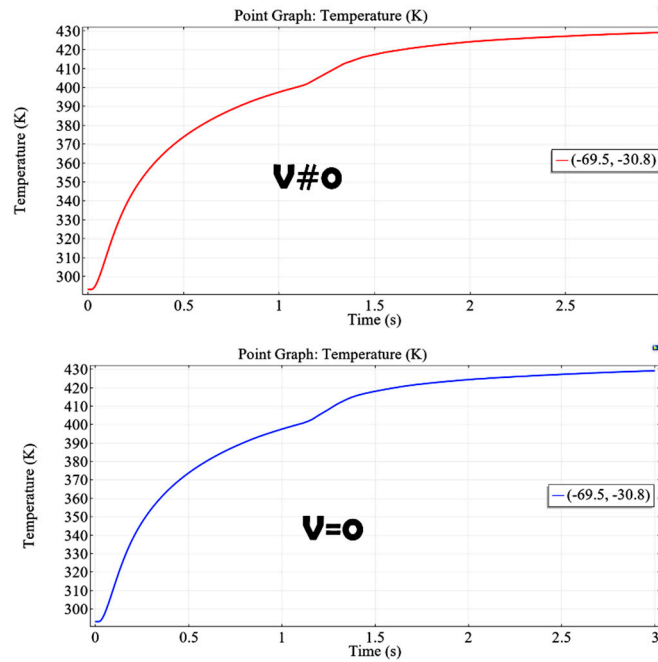


Figure S6. Graph of the temperature VS time at $v\#0$ and $V=0$

2.4 Dynamic heat transfer with increasing temperature along the top and bottom walls based on the approximative model of single-phase flow.

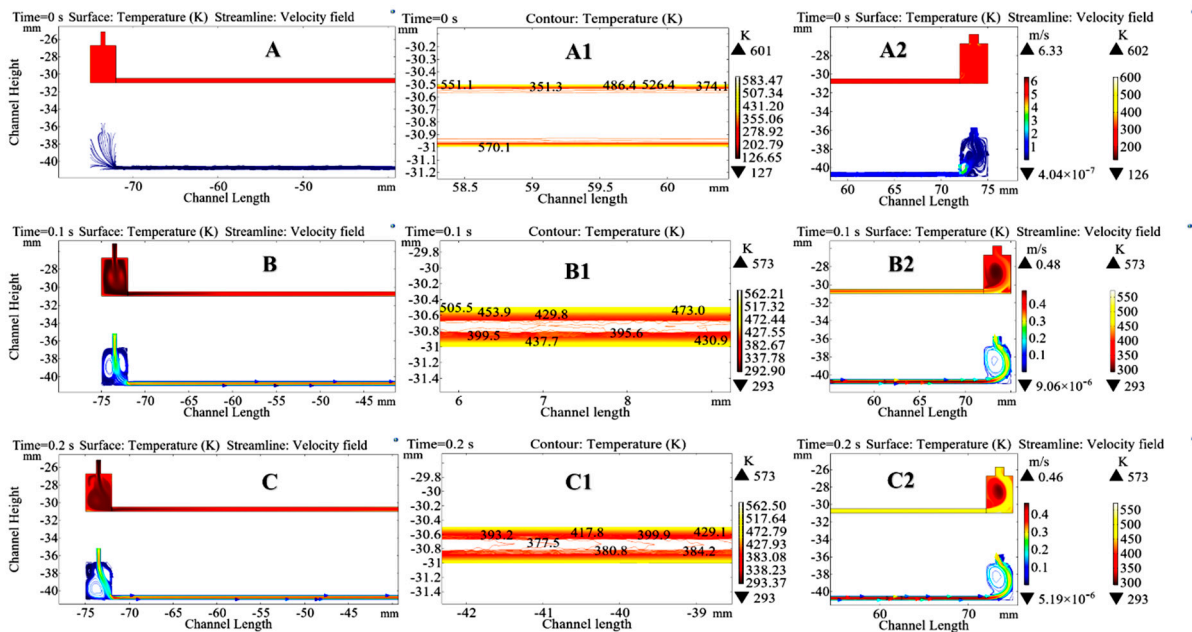


Figure S7. Dynamic of heat transfer of fluids with increasing temperature at the top and bottom side of the channel at the different operating time from $t = 0$ s to $t = 0.2$ s. [A-B-C] inlet of the channel, [A1-B1-C1] Isothermal contour of one portion of the channel along with the horizontal position (values are plotted randomly), [A2-B2-C2] Outlet of the channel. (no wall materials).

At $t = 0$ s; Figure S7 [A-A2] shows that the distribution of temperature and velocity is consistent in the channels from inlet to outlet. The water near the wall has a higher temperature indicated by the yellow color in [A1] Figure S7. The detailed temperature data along the horizontal direction at different positions of the channel, as shown in Table S7.

Table S7. Data along the channel at different horizontal positions.

Case 2: Dynamic heat transfer with increasing temperatures along the top and bottom walls						
Time: 0s						
Position (mm)	A: X= -71 Y=-30.8	B: X=-41 Y= -30.8	C: X= 10 Y= -30.8	D: X= 31 Y=-30.8	E: X= 61 Y=-30.8	F: X= 72.4 Y=-30.8
Temperature (K)	293.15	293.15	293.15	293.15	293.15	293.15
Time: 0.1s						
Position (mm)	A: X= -71 Y=-30.8	B: X= -41 Y= -30.8	C: X= -1 Y= -30.8	D: X= 31 Y=-30.8	E: X=61 Y=-30.8	F: X= 72.4 Y=-30.8
Temperature (K)	295.23	365.78	389.19	404.14	417.25	426.10
Time : 0.20s						
Position (mm)	A : X= -71 Y= -30.8	B: X= -41 Y= -30.8	C: X= -1 Y= -30.8	D: X= 31 Y=-30.8	E: X= 61 Y=-30.8	F: X= 72.4 Y=-30.8
Temperature (K)	306.69	377.5	438.91	462	483.60	494.28

At $t = 0.1s$; Figure S7 [B-B2] testifies that there is a small change of temperature and velocity in the mini-channel. The fluid penetrates the entire mini-channel with a fairly considerable velocity at its center marked by an orange color. The temperature of the walls is still hot but decreases because the fluid partially transports the heat during its passage in the channel. At a distance of about 30mm at the entrance to the channel, the walls are less hot because the fluid penetrates the canal. This cold fluid gradually spreads towards the warm parts of the channel due to the velocity, and there is a difference in coloration from the inlet to the outlet of the channel. The portion of the contour isothermal channel [B1] in Figure S7 indicates that the temperature varies from 295.23K to 426.10K, as presented in Table S7.

At $t = 0.20s$; Figure S7 [C-C2] attests a large change of temperature distribution in the horizontal mini-channel. The yellow coloration at the outlet in [C2] shows that the heat removed from the channel is considerable because of the fluid moves with a velocity of about 0.4 m / s as indicated by the orange coloration in its center and a velocity of about 0.3 m / s yellow-colored at the outlet [C2]. The portion of the contour isothermal channel in Figure S7 [C1] indicates that the temperature varies from 306.69K to 494.28K. Based on these values, the gradient temperature is operational, and the cooling is effective in the mini-channel.

References

1. Deepak, K.; Varma, V.B.; Prasanna, G.; Ramanujan, R.V. Hybrid thermomagnetic oscillator for cooling and direct waste heat conversion to electricity. *Applied Energy* **2019**, *233–234*, 312–320, doi:10.1016/j.apenergy.2018.10.057.
2. Pattanaik, M.S.; Varma, V.B.; Cheekati, S.K.; Prasanna, G.; Sudharsan, N.M.; Ramanujan, R.V. A self-regulating multi-torus magneto-fluidic device for kilowatt level cooling. *Energy Conversion and Management* **2019**, *198*, 111819, doi:10.1016/j.enconman.2019.111819.
3. Ganapathy, H.; Shooshitari, A.; Choo, K.; Dessiatoun, S.; Alshehhi, M.; Ohadi, M. Volume of fluid-based numerical modeling of condensation heat transfer and fluid flow characteristics in microchannels. *International Journal of Heat and Mass Transfer* **2013**, *65*, 62–72, doi:10.1016/j.ijheatmasstransfer.2013.05.044.

4. Özdemir, M.R.; Mahmoud, M.M.; Karayiannis, T.G. Flow Boiling of Water in a Rectangular Metallic Microchannel. *Heat Transfer Engineering* **2020**, 1–25, doi:10.1080/01457632.2019.1707390.
5. Li, M.; Bolotnov, I.A. Interface Tracking Simulation of Phase-Change Phenomena: Boiling and Condensation Verification. In Proceedings of the Volume 1A, Symposia: Turbomachinery Flow Simulation and Optimization; Applications in CFD; Bio-Inspired and Bio-Medical Fluid Mechanics; CFD Verification and Validation; Development and Applications of Immersed Boundary Methods; DNS, LES and Hybrid RANS/LES Methods; Fluid Machinery; Fluid-Structure Interaction and Flow-Induced Noise in Industrial Applications; Flow Applications in Aerospace; Active Fluid Dynamics and Flow Control — Theory, Experiments and Implementation; American Society of Mechanical Engineers: Washington, DC, USA, 2016; p. V01AT06A001.
6. Zhuan, R.; Wang, W. Flow pattern of boiling in micro-channel by numerical simulation. *International Journal of Heat and Mass Transfer* **2011**, S0017931011006661, doi:10.1016/j.ijheatmasstransfer.2011.11.029.
7. Hamami, A. Simulation de l'écoulement dans un minicanal. PhD Thesis, Université de Batna 2, Fesdis, Algeria, 2005.
8. Hassinet, L'Etude De L'écoulement Laminaire Dans Un Minicanal Par La Méthode Des Volumes Finis. PhD Thesis, Université de Batna 2, Fesdis, Algeria, 2008.
9. Peng, X.F.; Peterson, G.P.; Wang, B.X. Frictional flow characteristics of water flowing through rectangular microchannels. *Experimental Heat Transfer An International Journal* **1994**, 7, 249–264.
10. Bricard, A. Ecoulement et transfert de chaleur dans les microcanaux et dans les microcaloducs. STI/LASP 95.01, CENG/CEA Grenoble, France, 1995
11. Peng, X.F.; Peterson, G.P. Convective heat transfer and flow friction for water flow in microchannel structures. *International journal of heat and mass transfer* **1996**, 39, 2599–2608.
12. Kandlikar, S.; Garimella, S.; Li, D.; Colin, S.; King, M.R. *Heat transfer and fluid flow in minichannels and microchannels*; elsevier, 2005;
13. Gradeck, M. Structure de l'écoulement diphasique gaz-liquide dans les échangeurs à plaques corruguées. PhD Thesis, Nancy 1, 1 Rue Grandville 54000 Nancy, 1996.
14. Lide, D.R. *CRC handbook of chemistry and physics*; CRC press: Boca Raton, 2004; Vol. 85.
15. Holman, J.P. *Heat transfer*; McGraw-Hill, Avenue of the Americas, New York, USA, 2010.
16. Phillips, R.J. Microchannel heat sinks. *The Lincoln Laboratory Journal* **1988**, 1, 31–48.



© 2020 by the authors. Licensee MDPI, Basel, Switzerland. This article is an open access article distributed under the terms and conditions of the Creative Commons Attribution (CC BY) license (<http://creativecommons.org/licenses/by/4.0/>).